Science Advances
AAAS

Supplementary Materials for

The ins and outs of membrane bending by intrinsically disordered proteins

Feng Yuan *et al.*

Corresponding author: Jeanne C. Stachowiak, jcstach@austin.utexas.edu;
Padmini Rangamani, prangamani@ucsd.edu

Sci. Adv. **9**, eadg3485 (2023)
DOI: 10.1126/sciadv.adg3485

This PDF file includes:

Supplementary Figures

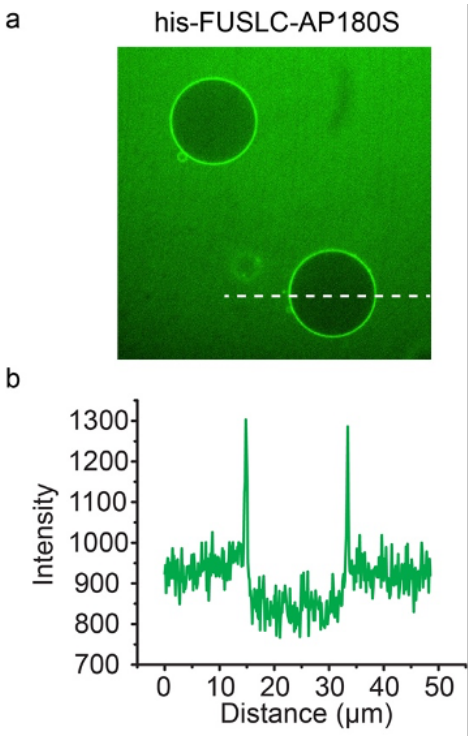

Figure S1. (a) Representative confocal images showing protein exclusion from the inner lumen of GUVs. (b) Intensity distribution of protein channel along the dashed line shown in the image.

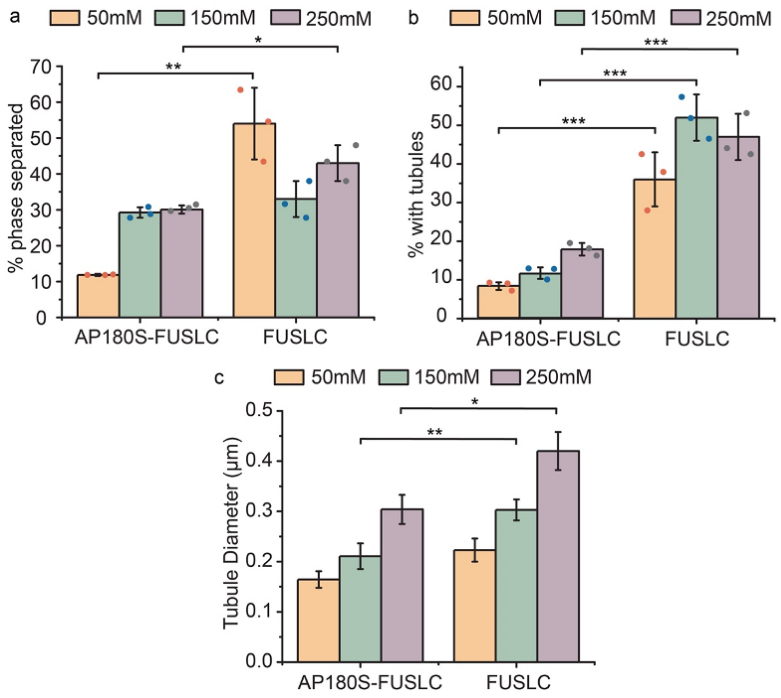

Figure S2. Bar chart comparison of percentage of GUVs displaying protein phase separation (a), inward tubules (b) and average inward tubule diameter (c) when incubated with his-AP180S-FUSLC and his-FUSLC under different salt concentrations. The data for his-FUSLC are cited from our previous report (*12*). Error bars in (a) and (b) represent the standard deviation of three independent trials (indicated by the dots). Error bars in (c) correspond to standard error of all data points measured under each condition. Statistical significance was tested using an unpaired, two-tailed student's t test. *: $P < 0.05$, **: $P < 0.01$, ***: $P < 0.001$. GUV composition is 83 mol% POPC, 15 mol% DGS-NTA-Ni, 2 mol% DP-EG10 biotin, and 0.1 mol% Texas Red-DHPE.

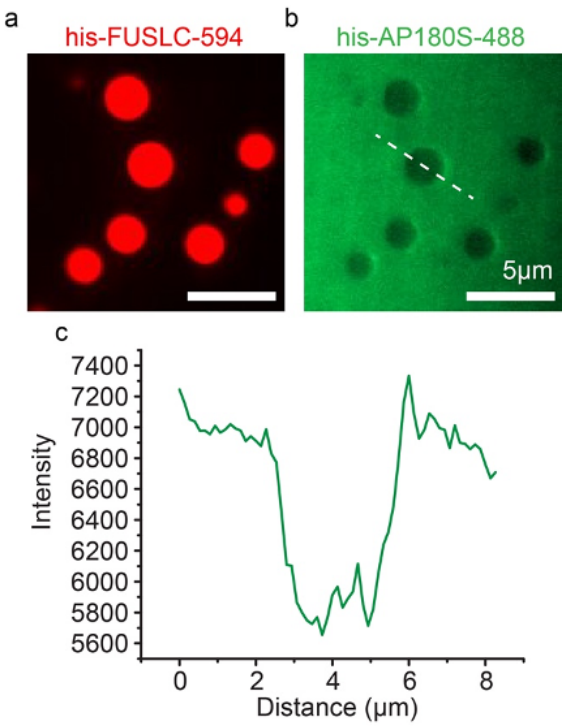

Figure S3. (a, b) Representative image of AP180S exclusion from his-FUSLC droplets in solution. (c) Intensity distribution of his-AP180S along the white dashed line across the his-FUSLC droplet in panel b. his-FUSLC concentration is 25 μM and his-AP180S is 5 μM. Experiment was done in 25mM HEPES, 150mM NaCl, pH 7.4 buffer.

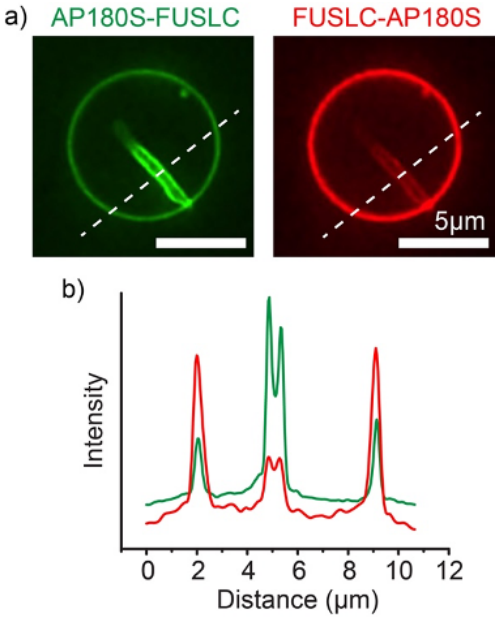

Figure S4. AP180S-FUSLC is more enriched in the inward protein-lined tubules than FUSLC-AP180S. (a) Representative super-resolution images of protein-lined tubules when GUVs were incubated with 1 μM of his-AP180S-FUSLC and 0.1 μM of his-FUSLC-AP180S at the same time. (b) Intensity distribution along the dashed line across the GUV.

Supplementary Information about Simulations

To the first order, the total system energy can be written as:

$W_{total} = W_{protein} + W_{membrane} = F_{brush}H + \kappa(H - c_0)^2$ Equation S1

where F_{brush} is the protein energy density, H is the mean curvature of the membrane, κ is the bending modulus, and c_0 the spontaneous curvature. The first term, the product of protein energy density and mean curvature, captures the moment arm generated by the protein steric interactions which are offset from the membrane surface. The second term is the conventional Helfrich-Canham-Evans hamiltonian which captures the membrane's bending elasticity. (*25-27*)

The physics of interacting polymers grafted on surfaces has been explored in detail and the brush polymer theory has been developed to model the contributions to the polymer energy density (*21-24*). Following the theory, the protein energy density, F brush, is defined as,

$F_{brush} = F_{elastic\ stretching} + F_{interactions} + F_{ion} = k_BTs[\frac{3}{2a^2s^2c} + Ac^2 + \frac{\alpha^2c^2}{2\Phi}]$ Equation S2

where s is the local area per protein, a is the Kuhn length, c the protein monomer concentration (considered to be an amino acid residue for the IDPs of interest), A the second virial coefficient, Φ the bulk ionic concentration, k_BT is the Boltzmann constant and temperature, and α the degree of ionization. While a freely jointed polymer chain is expected to form a glob like structure which maximizes its configurational entropy (*43*), high density packing conveyed by the area occupancy and protein concentration, can lead to stretching and subsequent entropy loss which is captured by the first term. The free energy density of the short-ranged interactions which can drive phenomena such as steric pressure and condensation is modeled by the virial expansion truncated to second order, the second term of Eq. S2. Here we note that A, the second virial coefficient, is a complex function of the specific protein chemistry/identity (*44, 45*) and can take a positive or negative value corresponding to repulsive or attractive behavior respectively. Conventional biochemistry and statistical mechanics further imply that A is a function of the local chemical environment which can screen the strength of interactions. In lieu of detailed experimental characterization of A given the combinatorial conditions, we will instead systematically vary the value of A across a range of values corresponding to net protein attraction/aggregation and repulsion. The third term of Eq. S2, captures the loss of entropy of ions partitioning into the brush layer as a result of Donnan's equilibrium. From the brush polymer theories, this term corresponds to the so-called quenched or strongly dissociating condition which assumes that the polymer has a fixed ionization extent given by α.

To interrogate how the IDP layer and membrane couple to drive spontaneous curvature we can study how the energy of the system changes with respect to changing mean curvature, $\partial W/\partial H$. The stationary point where $\frac{\partial W}{\partial H} = 0$, corresponds to the minima and is given by

$\frac{\partial W}{\partial H} = F_{brush} + 2\kappa c_0 = 0$ Equation S3

Rearranging, we obtain the classic relationship linking the moment of the protein interactions with the spontaneous curvature and bending rigidity,
$-2\kappa c_0 = F_{brush}$.

For a quantitative evaluation of this relationship, we further assume and prescribe values for the parameters. The Kuhn length, a, is twice the persistence length of a polymer. For an IDP we approximate this as twice the length of a residue, ~1 nm. (*46*) To relate the end-to-end stretch distance of the grafted IDP (i.e., thickness of the brush layer), d, to polymer area occupancy we write a conservation equation,

$s = \frac{N}{dc_p}$ Equation S4

where N is the number of amino acids, and c_p is the protein monomer concentration. We further assume that the degree of ionization for each protein is around 10%, $\alpha = 0.1$, the brush layer is 20 nm thick, and prescribe 150 mM ion concentration. Under these conditions we vary the second virial coefficient, A, from -10 – 10 nm^3 corresponding to net attractive (e.g., FUSLC) and repulsive (e.g., AP180S) conditions respectively. We find that the extent of spontaneous curvature induced is a function of protein concentration in line with the experimental observations, Figure 6b.

To evaluate how the spontaneous curvature influences the geometry of a membrane tube, we followed the approach outlined by Shurer, Derenyi and colleagues (*9, 47*). Considering the special case of a cylindrical membrane tube experiencing a pulling force at zero osmotic pressure, the Helfrich-Canham-Evans free energy is given by,

$W_{cyl} = [\frac{\kappa}{2}(\frac{1}{R} - c_0)^2 + \sigma]2\pi RL - fL$ Equation S5

where κ is the bending modulus, R is the radius of the cylinder, c_0 is the spontaneous curvature, σ is the tension, f is the pulling force acting over length L. At equilibrium, where $\frac{\partial W_{cyl}}{\partial R} = 0$ and $\partial W_{cyl}/\partial L = 0$, the tube radius is

$R = \frac{1}{\sqrt{{c_0}^2 + 2\sigma/\kappa}}$ Equation S6

and the pulling force,

$f = 2\pi\kappa(\sqrt{{c_0}^2 + 2\sigma\kappa} - c_0)$ Equation S7

Assuming a canonical bending rigidity value of 20 k_BT and membrane tension 0.01 mNm^{-1}, and substituting the predicted values from Figure 6b, we obtain the radius and force predictions in Figure 6c and Figure S5.

For a proof of principle of inward and outward tube formation with pearling, we used Mem3DG (*28*) to build a model in three dimensions without assumptions of axisymmetry. Mem3DG is a

framework and simulation engine that enables us to solve the governing equations of membrane bending. Using principles from discrete differential geometry, we compute the energy of a geometric configuration and vertexwise forces in a consistent manner with traditional physics approaches; coupled with an energy minimization or time integration scheme, we get from the model a trajectory of the evolving domain subject to the bending and other prescribed physics. For the demonstration, we start from a spherical vesicle and apply a weak Gaussian point force, decaying in time, in an inward or outward direction to induce initial tube formation. Proteins which impart spontaneous curvature matching the direction of the tube bind and support the extrusion of pearls. Driven by the membrane tension and protein spontaneous curvature, the resulting configurations, shown in Figure 6d, exhibit pearled tubules similar to those observed in experiments, (Figure 2c, 4c) suggesting that our simple physical model captures the main features of our experimental system.

All parameters for the Mem3DG and simple mechanical models are archived on GitHub: https://github.com/RangamaniLabUCSD/2023-IDP-bending. Mem3DG source code corresponding to commit 361affa9423d44f3cf239585ac350340a212b1f8 used to run the model can also be obtained from GitHub https://github.com/RangamaniLabUCSD/Mem3DG/.

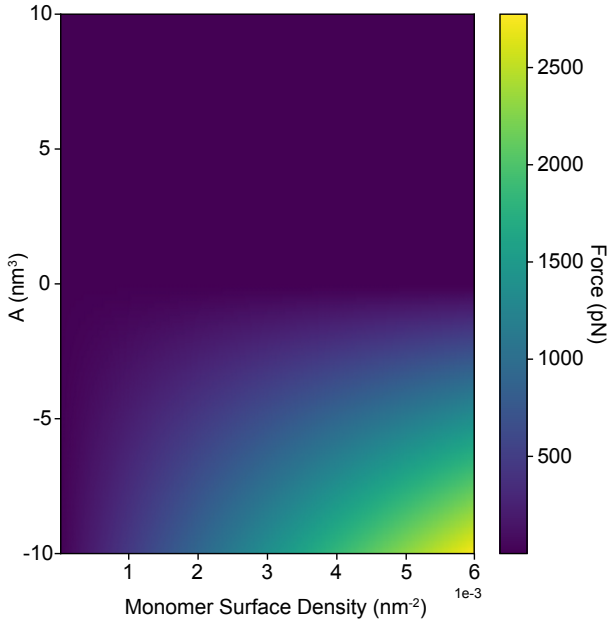

Figure S5. The equilibrium pulling force required to sustain a tube coated by differing surface concentrations of protein. The vertical axis is the second virial coefficient, A, which represents the net attraction—repulsion of the protein.

REFERENCES AND NOTES

1. H. T. McMahon, E. Boucrot, Membrane curvature at a glance. *J. Cell Sci.* **128**, 1065–1070 (2015).

2. I. K. Jarsch, F. Daste, J. L. Gallop, Membrane curvature in cell biology: An integration of molecular mechanisms. *J. Cell Biol.* **214**, 375–387 (2016).

3. J. H. Hurley, E. Boura, L.-A. Carlson, B. Różycki, Membrane budding. *Cell* **143**, 875–887 (2010).

4. G. Drin, B. Antonny, Amphipathic helices and membrane curvature. *FEBS Lett.* **584**, 1840–1847 (2010).

5. O. Daumke, A. Roux, V. Haucke, BAR domain scaffolds in dynamin-mediated membrane fission. *Cell* **156**, 882–892 (2014).

6. W. T. Snead, J. C. Stachowiak, Structure versus stochasticity-the role of molecular crowding and intrinsic disorder in membrane fission. *J. Mol. Biol.* **430**, 2293–2308 (2018).

7. D. J. Busch, J. R. Houser, C. C. Hayden, M. B. Sherman, E. M. Lafer, J. C. Stachowiak, Intrinsically disordered proteins drive membrane curvature. *Nat. Commun.* **6**, 7875 (2015).

8. W. T. Snead, W. F. Zeno, G. Kago, R. W. Perkins, J. B. Richter, C. Zhao, E. M. Lafer, J. C. Stachowiak, BAR scaffolds drive membrane fission by crowding disordered domains. *J. Cell Biol.* **218**, 664–682 (2019).

9. C. R. Shurer, Joe Chin-Hun Kuo, La Deidra Monét Roberts, J. G. Gandhi, M. J. Colville, T. A. Enoki, H. Pan, J. Su, J. M. Noble, M. J. Hollander, John P O'Donnell, R. Yin, K. Pedram, L. Möckl, L. F. Kourkoutis, W E Moerner, C. R. Bertozzi, G. W. Feigenson, H. L. Reesink, M. J. Paszek, Physical principles of membrane shape regulation by the glycocalyx. *Cell* **177**, 1757–1770.e21 (2019).

10. Clifford P. Brangwynne, P. Tompa, Rohit V. Pappu, Polymer physics of intracellular phase transitions. *Nat. Phys.* **11**, 899–904 (2015).

11. S. Boeynaems, S. Alberti, N. L. Fawzi, T. Mittag, M. Polymenidou, F. Rousseau, J. Schymkowitz, J. Shorter, B. Wolozin, L. Van Den Bosch, P. Tompa, M. Fuxreiter, Protein phase separation: A new phase in cell biology. *Trends Cell Biol.* **28**, 420–435 (2018).

12. F. Yuan, H. Alimohamadi, B. Bakka, A. N. Trementozzi, K. J. Day, N. L. Fawzi, P. Rangamani, J. C. Stachowiak, Membrane bending by protein phase separation. *Proc. Natl. Acad. Sci. U.S.A.* **118**, e2017435118 (2021).

13. E. W. Martin, A. S. Holehouse, I. Peran, M. Farag, J. J. Incicco, A. Bremer, C. R. Grace, A. Soranno, R. V. Pappu, T. Mittag, Valence and patterning of aromatic residues determine the phase behavior of prion-like domains. *Science* **367**, 694–699 (2020).

14. W. F. Zeno, A. S. Thatte, L. Wang, W. T. Snead, E. M. Lafer, J. C. Stachowiak, Molecular mechanisms of membrane curvature sensing by a disordered protein. *J. Am. Chem. Soc.* **141**, 10361–10371 (2019).

15. K. A. Burke, A. M. Janke, C. L. Rhine, N. L. Fawzi, Residue-by-residue view of in vitro FUS granules that bind the C-terminal domain of RNA polymerase II. *Mol. Cell* **60**, 231–241 (2015).

16. J. C. Stachowiak, E. M. Schmid, C. J. Ryan, H. S. Ann, D. Y. Sasaki, M. B. Sherman, P. L. Geissler, D. A. Fletcher, C. C. Hayden, Membrane bending by protein-protein crowding. *Nat. Cell Biol.* **14**, 944–949 (2012).

17. J. C. Stachowiak, C. C. Hayden, D. Y. Sasaki, Steric confinement of proteins on lipid membranes can drive curvature and tubulation. *Proc. Natl. Acad. Sci. U.S.A.* **107**, 7781–7786 (2010).

18. M. I. Angelova, A.-F. Bitbol, M. Seigneuret, G. Staneva, A. Kodama, Y. Sakuma, T. Kawakatsu, M. Imai, N. Puff, pH sensing by lipids in membranes: The fundamentals of pH-driven migration, polarization and deformations of lipid bilayer assemblies. *Biochim. Biophys. Acta Biomembr.* **1860**, 2042–2063 (2018).

19. S. Elbaum-Garfinkle, Y. Kim, K. Szczepaniak, C. C.-H. Chen, C. R. Eckmann, S. Myong, C. P. Brangwynne, The disordered P granule protein LAF-1 drives phase separation into droplets with tunable viscosity and dynamics. *Proc. Natl. Acad. Sci. U.S.A.* **112**, 7189–7194 (2015).

20. B. S. Schuster, E. H. Reed, R. Parthasarathy, C. N. Jahnke, R. M. Caldwell, J. G. Bermudez, H. Ramage, M. C. Good, D. A. Hammer, Controllable protein phase separation and modular recruitment to form responsive membraneless organelles. *Nat. Commun.* **9**, 2985 (2018).

21. E. Zhulina, T. Birshtein, O. Borisov, Curved polymer and polyelectrolyte brushes beyond the Daoud-Cotton model. *Eur. Phys. J. E Soft Matter.* **20**, 243–256 (2006).

22. R. Israels, F. Leermakers, G. J. Fleer, E. B. Zhulina, Charged polymeric brushes: Structure and scaling relations. *Macromolecules* **27**, 3249–3261 (1994).

23. O. Borisov, E. Zhulina, Effect of salt on self-assembly in charged block copolymer micelles. *Macromolecules* **35**, 4472–4480 (2002).

24. E. Zhulina, O. Borisov, Polyelectrolytes grafted to curved surfaces. *Macromolecules* **29**, 2618–2626 (1996).

25. E. Evans, R Skalak, Mechanics and thermodynamics of biomembranes: Part 2. *CRC Crit. Rev. Bioeng.* **3**, 331–418 (1979).

26. P. B. Canham, The minimum energy of bending as a possible explanation of the biconcave shape of the human red blood cell. *J. Theor. Biol.* **26**, 61–81 (1970).

27. E. A. Evans, Bending resistance and chemically induced moments in membrane bilayers. *Biophys. J.* **14**, 923–931 (1974).

28. C. Zhu, C. T. Lee, P. Rangamani, Mem3DG: Modeling membrane mechanochemical dynamics in 3D using discrete differential geometry. *Biophys. Rep.* **2**, 100062 (2022).

29. J. Zimmerberg, M. M. Kozlov, How proteins produce cellular membrane curvature. *Nat. Rev. Mol. Cell Biol.* **7**, 9–19 (2006).

30. H. T. McMahon, J. L. Gallop, Membrane curvature and mechanisms of dynamic cell membrane remodelling. *Nature* **438**, 590–596 (2005).

31. V. N. Uversky, Intrinsically disordered proteins and their “Mysterious” (Meta) Physics. *Front. Phys.* **7**, 10 (2019).

32. B. Xue, A. K. Dunker, V. N. Uversky, Orderly order in protein intrinsic disorder distribution: Disorder in 3500 proteomes from viruses and the three domains of life. *J. Biomol. Struct. Dyn.* **30**, 137–149 (2012).

33. D. J. Owen, B. M. Collins, P. R. Evans, Adaptors for clathrin coats: Structure and function. *Annu. Rev. Cell Dev. Biol.* **20**, 153–191 (2004).

34. P. Gómez-Puertas, C. Albo, E. Pérez-Pastrana, A. Vivo, A. Portela, Influenza virus matrix protein is the major driving force in virus budding. *J. Virol.* **74**, 11538–11547 (2000).

35. D. Saletti, J. Radzimanowski, G. Effantin, D. Midtvedt, S. Mangenot, W. Weissenhorn, P. Bassereau, M. Bally, The Matrix protein M1 from influenza C virus induces tubular membrane invaginations in an *in vitro* cell membrane model. *Sci. Rep.* **7**, 40801 (2017).

36. C. Strambio-De-Castillia, M. Niepel, M. P. Rout, The nuclear pore complex: Bridging nuclear transport and gene regulation. *Nat. Rev. Mol. Cell Biol.* **11**, 490–501 (2010).

37. M. P. Rout, J. D. Aitchison, A. Suprapto, K. Hjertaas, Y. Zhao, B. T. Chait, The yeast nuclear pore complex: Composition, architecture, and transport mechanism. *J. Cell Biol.* **148**, 635–652 (2000).

38. D. P. Denning, S. S. Patel, V. Uversky, A. L. Fink, M. Rexach, Disorder in the nuclear pore complex: The FG repeat regions of nucleoporins are natively unfolded. *Proc. Natl. Acad. Sci. U.S.A.* **100**, 2450–2455 (2003).

39. N. Nag, S. Sasidharan, V. N. Uversky, P. Saudagar, T. Tripathi, Phase separation of FG-nucleoporins in nuclear pore complexes. *Biochim. Biophys. Acta Mol. Cell Res.* **1869**, 119205 (2022).

40. N. Momin, S. Lee, A. K. Gadok, D. J. Busch, G. D. Bachand, C. C. Hayden, J. C. Stachowiak, D. Y. Sasaki, Designing lipids for selective partitioning into liquid ordered membrane domains. *Soft Matter* **11**, 3241–3250 (2015).

41. M. I. Angelova, D. S. Dimitrov, Liposome electroformation. *Faraday Discuss. Chem. Soc.* **81**, 303–311 (1986).

42. W. F. Zeno, U. Baul, W. T. Snead, A. C. M. DeGroot, L. Wang, E. M. Lafer, D. Thirumalai, J. C. Stachowiak, Synergy between intrinsically disordered domains and structured proteins amplifies membrane curvature sensing. *Nat. Commun.* **9**, 4152 (2018).

43. O. Kratky, G. Porod, Röntgenuntersuchung gelöster fadenmoleküle. *Recueil des Travaux Chimiques des Pays-Bas* **68**, 1106–1122 (1949).

44. B. Neal, D. Asthagiri, A. Lenhoff, Molecular origins of osmotic second virial coefficients of proteins. *Biophys. J.* **75**, 2469–2477 (1998).

45. A. Quigley, D. Williams, The second virial coefficient as a predictor of protein aggregation propensity: A self-interaction chromatography study. *Eur. J. Pharm. Biopharm.* **96**, 282–290 (2015).

46. U. B. Choi, J. J. McCann, K. R. Weninger, M. E. Bowen, Beyond the random coil: Stochastic conformational switching in intrinsically disordered proteins. *Structure* **19**, 566–576 (2011).

47. I. Derényi, F. Jülicher, J. Prost, Formation and interaction of membrane tubes. *Phys. Rev. Lett.* **88**, 238101 (2002).